

Mapping Driven Oscillations in the Size of a Bubble to the Dynamics of a Newtonian Particle in a Potential

Uri Shimon¹ and Ady Stern¹

Department of Condensed Matter Physics, Weizmann Institute of Science, Rehovot 76100, Israel

(*Electronic mail: u.shimon@weizmann.ac.il)

(Dated: 11 September 2024)

The non-linear dynamics of driven oscillations in the size of a spherical bubble are mapped to the dynamics of a *Newtonian particle in a potential* within the incompressible liquid regime. The compressible liquid regime, which is important during the bubble's sonic collapse, is approached adiabatically. This new framework naturally distinguishes between the two time scales involved in the non-linear oscillations of a bubble. It also explains the experimentally observed sharp rebound of the bubble upon collapse. Guided by this new vantage point, we develop analytical approximations for several key aspects of bubble motion. First, we formulate a tensile strength law that integrates the bubble's ideal gas behavior with a general polytropic index. Next, we derive an acoustic energy dissipation formula for the bubble's sonic collapse, dependent solely on the bubble's collapse radii and velocity. Finally, we establish a straightforward physical criterion for Bjerknes force reversal, governed by the driving pressure, ambient pressure and tensile strength.

Keywords: bubble dynamics, sonoluminescence, cavitation, Rayleigh-Plesset equation, Keller-Herring equation

I. INTRODUCTION

Spherical micro bubble collapse can lead to immense energy-per-particle focusing of almost 12 orders of magnitude, leading to light emission known as *sonoluminescence*¹⁻⁹. The shock wave generated in the process has associated pressures on the order of GPa¹⁰⁻¹². Such pressures possess a high damaging power that can wear metallic surfaces and is a major concern in the design of ship propellers^{13,14}, hydraulic turbines¹⁵, artificial heart valves¹⁶ and liquid-propelled rocket engines¹⁷⁻¹⁹. It is also used by the mantis shrimp in the killing of its prey^{20,21}. The damaging power can be used in various novel medical applications²² (e.g., shock wave lithotripsy²³⁻²⁵ and cancer therapy^{22,26}) and for water treatment²⁷⁻²⁹.

In the presence of an oscillating acoustic field, the bubble collapse can be made periodic, encompassing two distinct time scales: the *slow* driving frequency measured in kHz, and the *fast* MHz oscillations that arise post the initial collapse of the bubble (referred to as "after bounces")¹⁻⁴, see Fig. 2. It also spans a broad range of length scales, from 0.1 to 10 μm .

The dynamics of a spherical bubble with radius $R(t)$ in the incompressible fluid regime are described by the well-known Rayleigh-Plesset equation³⁰⁻³⁴:

$$R\ddot{R} + \frac{3}{2}\dot{R}^2 = \frac{p_{GE} \left(\frac{R_{E0}}{R}\right)^{3k} + p_V - p_0 - p_d(t)}{\rho_L} - \frac{4v_L}{R}\dot{R} - \frac{2S}{\rho_L R} \quad (1)$$

The bubble is treated as an ideal gas going through a polytropic process with index k , p_{GE} being the reference pressure at the ambient equilibrium radius, R_{E0} , S is the surface tension and p_V, p_0 are the vapor and ambient pressures, respectively. The driving pressure, $p_d(t)$, is the oscillatory pressure associated with the acoustic wave, characterized by

the frequency ω_d . We will refer to the pressure difference $\Delta p(t) \equiv p_V - p_0 - p_d(t)$ as the tension. The tensile strength is the critical tension, Δp_c , at which significant bubble expansion takes place³³.

For an oscillating bubble in sonoluminescence conditions, the incompressibility of the liquid is a sensible assumption throughout the entire motion of the bubble, except during the bubble's sonic collapse^{1,35}. Perturbation theory in the bubble's Mach number ($M \equiv \frac{\dot{R}}{c}$) can be used to extend (1) to the *general* Keller-Herring equation, valid to first order in M ³⁵:

$$(1 - (\lambda + 1)M)R\ddot{R} + \left(1 - \frac{1}{3}(3\lambda + 1)M\right)\frac{3}{2}\dot{R}^2 = (1 + (1 - \lambda)M)h_B + \frac{R}{c}\dot{h}_B \quad (2)$$

where

$$h_B \equiv \frac{p_{GE} \left(\frac{R_{E0}}{R}\right)^{3k} + \Delta p(t) - \frac{2S}{R} - \frac{4v_L \rho_L}{R}\dot{R}}{\rho_L}$$

wherein c is the speed of sound in the liquid and λ is a positive, "tunable" parameter that must not exceed $\frac{1}{M}$; for $\lambda = 0$ equation (2) reduces to Keller's form³⁶⁻³⁸, and for $\lambda = 1$ it reduces to Herring's form^{39,40}.

The primary Bjerknes force is a translational force acting on an acoustically driven bubble. It is defined as the time-averaged product of the pressure gradient and the bubble's volume over an acoustic cycle, $\langle \nabla p R^3 \rangle$ ⁴¹⁻⁴⁴. In the presence of a *weak* standing acoustic wave, bubbles with a small ambient equilibrium radius are drawn towards the pressure antinodes, while those with a larger ambient equilibrium radius are drawn towards the nodes. Consequently, the Bjerknes force dictates the effective pressure a bubble experiences and plays a key role in defining the parameter space for stable sonoluminescence^{44,45}.

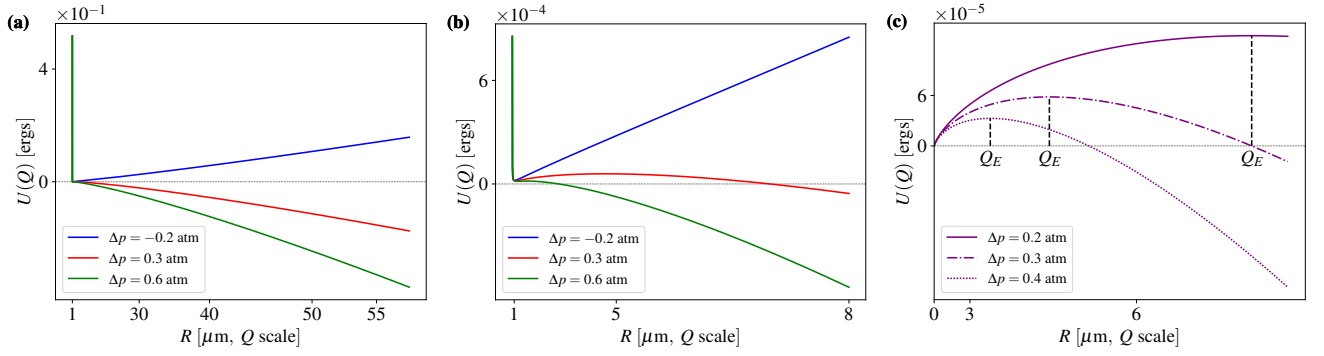


FIG. 1: The bubble's instantaneous potential in an incompressible fluid (Eq. (3), $Q_{E0} = 1 \mu\text{m}^{\frac{5}{3}}$, $S = 0.0728 \frac{\text{N}}{\text{m}}$) plotted in $Q = R^{\frac{5}{3}}$ scale. **(a)-(b)** The long and short range structure of the potential for $k = \frac{5}{3}$. For negative tension (the blue curve), a single stable equilibrium radius exists and the potential is binding. For positive tension (red and green curves), the potential is non-binding in the long range. However, if the tension is lower than the tensile strength (the red curve), a meta-stable equilibrium radius exists, with a locally binding potential around it. **(c)** The potential for $k < \frac{1}{3}$ and varying tension. The unstable equilibrium point, $Q_E(\Delta p)$, approaches zero as the tension is increased.

In this work, we transform the non-linear Rayleigh-Plesset equation to a linear equation of motion of a Newtonian particle in a potential. Our starting point is the transformation $Q = R^{\frac{5}{3}}$, introduced first in a more limited context by Childs⁴⁶. The transformation is extended to the compressible liquid regime by defining $X = R^{\frac{5}{3} + \frac{M}{1 - (\lambda - 1)M}}$ and using an adiabatic approach on the bubble's Mach number ($M \equiv \frac{\dot{R}}{c}$). This novel framework naturally distinguishes between the two time scales of the driven motion. The slow time scale is the acoustic period, while the fast time scale is the one associated with oscillations of the Newtonian particle within its potential. The potential, drawn in Fig. 1, manifests a very sharp wall at $Q \rightarrow 0$ for $k > \frac{1}{3}$. This sharp wall leads to very high acceleration at the bubble's rebound from its collapse, which is observed experimentally¹⁻³ (see Fig. (2)). It also indicates that such a rebound is not expected for $k < \frac{1}{3}$. Guided by our new vantage point, the tensile strength, $\Delta p_c \equiv (p_V - p_0 - p_d)_c$, at which significant bubble expansion is anticipated, is calculated, including its dependence on S and k ³³. Additionally, the acoustic energy dissipation during collapse is calculated as a function of the bubble's Mach number and its initial, final and equilibrium radii. Finally, a physical criterion for the reversal of the primary Bjerknes force is established, relying exclusively on the driving pressure, ambient pressure and tensile strength.

II. THE POTENTIAL IN THE INCOMPRESSIBLE REGIME

To map (1) to the dynamics of a Newtonian particle in a potential, we apply the transformation $Q = R^{\frac{5}{3}}$. This transforms Eq. (1) to an equation of motion of a non-relativistic particle subject to a time-dependent potential and a spatially varying

frictional force:

$$\rho_L \ddot{Q} = -\frac{d}{dQ} U_k(Q) - 4\rho_L \nu_L \frac{\dot{Q}}{Q^{\frac{4}{3}}} \quad (3)$$

where

$$U_k = \frac{25}{12} \left(\frac{p_{GE}}{(k-1)} \left(\frac{Q_{E0}}{Q} \right)^{\frac{6k}{5}} + p_0 + p_d(t) - p_V \right) Q^{\frac{6}{5}} + \frac{25}{4} S Q^{\frac{4}{5}} \quad (4)$$

wherein $Q_{E0} = R_{E0}^{\frac{5}{3}}$ denotes the ambient equilibrium point. For $k = 1$, the polytropic term changes to $-\frac{5}{2} p_{GE} Q_{E0}^{\frac{6}{5}} \log\left(\frac{Q}{Q_{E0}}\right)$. The resulting dynamics may take several qualitatively different forms, depending on the number and type of extremal points of $U_k(Q)$. This number is determined by the number of *positive* solutions of:

$$\partial_Q U_k(Q) = 0 \iff p_{GE} Q_{E0}^{\frac{6k}{5}} + \Delta p Q_E^{\frac{6k}{5}} = 2S Q_E^{\frac{6k-2}{5}} \quad (5)$$

We denote these solutions by Q_E .

The tensile strength, $\Delta p_c \geq 0$, can now be calculated, and to that end we consider now positive tension. For $k < \frac{1}{3}$, the potential has a single unstable equilibrium point which approaches 0 as the tension is increased (Fig. 1c). The bubble expands when its size is larger than its equilibrium point, which happens when the tension overcomes the surface tension:

$$\Delta p_c = \frac{2S}{Q_{E0}^{\frac{2}{3}}} - p_{GE} \left(k < \frac{1}{3} \right) \quad (6)$$

The tensile strength is then independent of k .

If $k > \frac{1}{3}$, for strong positive tension there will be no equilibrium point in the potential, as seen in the green curve in Fig.

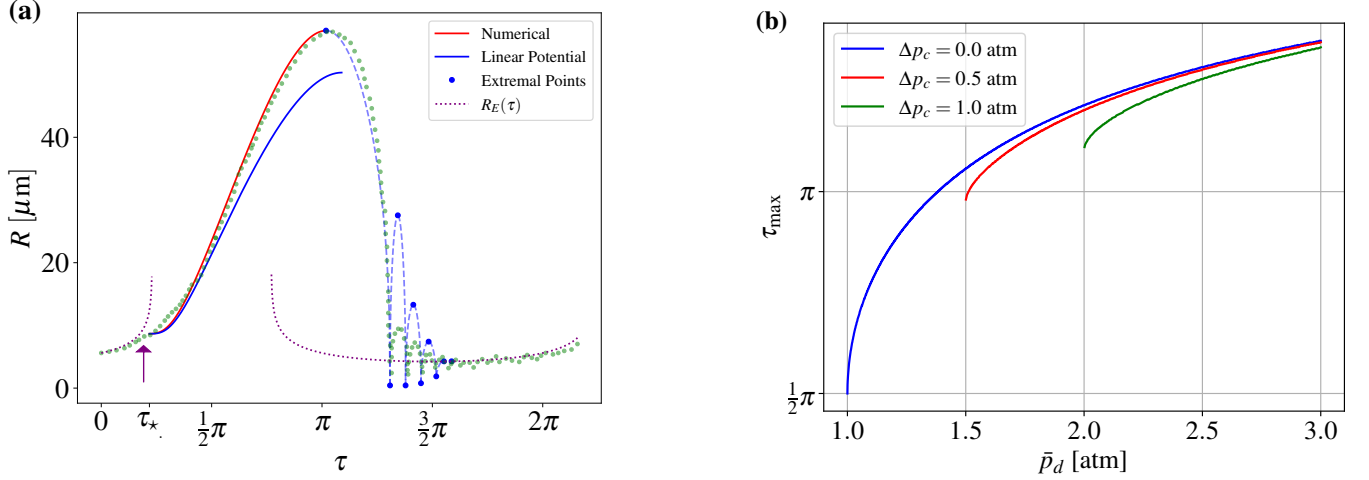


FIG. 2: **(a)** The bubble radius versus dimensionless time $\tau = \omega_d t$; The green dots are experimental data, adapted from Putterman and Weninger¹. Initially and as long as the equilibrium radius changes slowly (between $\tau = 0$ and the purple arrow), the bubble follows its equilibrium radius, $R_E(\tau)$, that is given by (8). The blue curve represents the bubble expansion under the influence of a linear potential (Eq. (9)) starting from τ_* , where the potential becomes non-binding. The red curve is obtained by numerically applying (9) to small time-segments, adding the effect of the change in Q . The collapse and after-bounces extremal points (the blue dots) were calculated using an iterative energy calculation outlined in Appendix C (with $M = -0.9$). **(b)** The phase at which the bubble reaches its maximal size, τ_{\max} , versus the driving amplitude, \bar{p}_d . The figure assumes the limit of strong bubble oscillations ($\bar{p}_d \geq \Delta p_c + (p_0 - p_V)$) and negligible velocity at τ_* . If $\tau_{\max} \geq \pi$ Bjerknes force reversal is expected to be important, see Section V.

1a-b. In contrast, for weak positive tension there will be one maximum and one minimum point to the potential, as seen in the red curve in Fig. 1b. The system is assumed to start in the weak tension regime, at the minimum point of the potential. The second derivative of the potential does not change sign in the strong tension case, but does go through zero in the weak tension case. Its examination, then, allows us to extract the tensile strength:

$$\Delta p_c = \frac{2(3k-1)}{3k} \left(\frac{2S^{3k}}{3k p_{GE} Q_{E0}^{\frac{6k}{5}}} \right)^{\frac{1}{3k-1}} \left(k > \frac{1}{3} \right) \quad (7)$$

The tensile strength is then k -dependent for $k > \frac{1}{3}$.

Treating the bubble expansion as an isothermal process with $k = 1$, transforms (5) to a cubic equation for $R_E \equiv Q_E^{\frac{2}{5}}$. When $\Delta p \in (-\Delta p_c, \Delta p_c)$ the solution is:

$$R_E = \frac{4S}{3\Delta p} \left\{ \frac{1}{2} + \cos \left[\frac{1}{3} \arccos \left(1 - 2 \left(\frac{\Delta p}{\Delta p_c} \right)^2 \right) - \frac{2\pi n_*}{3} \right] \right\} \quad (8)$$

where n_* is chosen such that R_E is the smallest positive root. The full solution is shown in Appendix A.

Strong oscillations of the bubble size ($\max Q \gg Q_{E0}$) thus require that at least at some part of the driving period $\Delta p(t) > \Delta p_c$.

Before concluding this section, we note that approximations which are often cited in the literature are written in the somewhat unnatural form: $R(t) = f(t)^{\frac{2}{5}}$ ^{6,47,48}. This arbitrarily looking form in the R frame has a clear meaning in the Q frame. The assumption $R(t) = (A + vt)^{\frac{2}{5}}$ is nothing but a free motion of the particle in the Q frame ($\dot{Q} = \text{const}$) whereas $R(t) = (A + at^2)^{\frac{2}{5}}$ corresponds to a motion with constant acceleration ($\ddot{Q} = \text{const}$).

III. THE ACOUSTIC CYCLE

In this section, we develop an analytical description of the bubble motion during one acoustic cycle by dividing it into segments.

We work in the driving time scale, $\tau = \omega_d t$, setting the bubble's initial conditions to $Q(\tau = 0) = Q_{E0}$ with some positive velocity and assuming that the driving takes the form $p_d(\tau) = -\bar{p}_d \sin(\tau)$.

As τ increases, the driving goes negative, raising the tension, $\Delta p(t)$, and the instantaneous equilibrium point begins to increase slowly, $Q_E(t)/\frac{dQ_E(t)}{dt} \ll \omega(Q_E, t)$. Where $\omega(Q_E, t)$ is the frequency of oscillations around the minimum of the potential (see Eq. (B2)). At this stage, the bubble follows the instantaneous equilibrium point and $Q(\tau) \approx Q_E(\tau)$. For isothermal processes, with $k = 1$, $Q_E(\tau)$ is analytically described by Eq. (8). It is plotted as a dotted purple curve in Fig. 2a. At some moment, the change in the equilibrium point is too fast, i.e., $Q_E(t)/\frac{dQ_E(t)}{dt} \sim \omega(Q_E, t)$, and the bubble can-

not follow it anymore. This instance is marked by the purple arrow in Fig. 2a.

Then, at $\tau_* = \arcsin\left(\frac{\Delta p_c + (\rho_0 - \rho_V)}{\bar{p}_d}\right)$, the tension is equal to the tensile strength, $\Delta p(\tau_*) = \Delta p_c$, and the bubble equilibrium radius ceases to exist. The potential is non-binding and as long as $\Delta p(\tau) > \Delta p_c$ the bubble expands. When $Q \gg Q_{E0}$, the ideal gas pressure and surface tension are minute compared to the tension term and the potential can be assumed to take the form $U(Q, t) \sim \Delta p(t)Q^{\frac{6}{5}}$. In this limit, we may get a good description of the dynamics if we approximate the potential to be linear (see Fig. 3). Under this approximation the force acting on the particle is Q -independent, but time-dependent. The solution to the equation $\ddot{Q} = -\Delta p(\tau)Q(\tau_*)^{\frac{1}{5}}$ may be expressed as a function of $\Delta\tau \equiv \tau - \tau_*$:

$$Q(\tau) = Q(\tau_*) + \alpha\Delta\tau^2 + \beta\Delta\tau + \gamma[\sin(\tau_* + \Delta\tau) - \sin(\tau_*)] \quad (9)$$

where α, β, γ are determined by the value of $\tau_*, Q(\tau_*)$ and $\left.\frac{dQ}{d\tau}\right|_{\tau=\tau_*}$ (the full form is shown in Eq. (B4)). Taking $Q(\tau_*)$ from the experimental data¹ and neglecting $\left.\frac{dQ}{d\tau}\right|_{\tau=\tau_*}$ the blue curve in Fig. 2a was obtained. The linear potential approximation demonstrates good accuracy in determining the phase in which the bubble reaches its maximal radius, τ_{\max} . This phase plays a major role in the reversal of the Bjerknes force^{42,43}. In Section V we utilize the analysis presented here to formulate a physical condition for the reversal of the Bjerknes force. Additionally, Fig. 2b shows τ_{\max} as a function of the driving pressure amplitude, \bar{p}_d , for various tensile strengths, Δp_c . The figure assumes the limit of strong bubble oscillations and negligible velocity at τ_* .

At τ_{\max} the bubble reaches its maximum size and is ready to begin its collapse. From this instance until the end of the acoustic cycle, the tension remains below the tensile strength, $\Delta p(\tau) < \Delta p_c$. The potential then becomes binding, and the bubble oscillates around its minimum. During the first oscillation, the bubble undergoes its primary collapse, reaching sonic velocities and experiencing significant damping due to the compressibility of the liquid. After the primary collapse, the bubble quickly rebounds, resulting in rapid, damped oscillations around the equilibrium point. These oscillations occur on a fast time scale and are known as "after bounces".

In Section IV we develop a formula for the acoustic energy dissipation during the bubble's sonic collapse (Eq. (18)). Using this formula, the after-bounces extremal points were calculated and plotted as blue points in Fig. 2a. Experimental data shows that around 99% of the energy is lost between the first and second maximum points of the oscillations. Acoustic dissipation that is included in our model accounts for around 90% of the energy loss, with the remaining energy loss accounted for by viscosity and luminescence¹, which are not included in the model.

IV. THE COMPRESSIBLE LIQUID REGIME

The compressibility of the liquid is important when the bubble undergoes its violent collapse^{1,6-9,35}. To account for it, the fairly complex Rayleigh-Plesset equation (1) has to be replaced by the even more complex *general* Keller-Herring equation (2). To extend our approach to this case, we modify the original transformation to:

$$X = R^{\alpha(M)} \quad (10)$$

where

$$\alpha(M) \equiv \frac{5}{2} + \frac{M}{1 - (\lambda + 1)M} \quad (11)$$

The kinetic energy in this case will be proportional to $R^D \dot{R}^2$, where D is the problem's *effective dimension*:

$$D(M) = 3 + \frac{2M}{1 - (\lambda + 1)M} \quad (12)$$

The compressibility of the liquid then changes the dimension of the Rayleigh-Plesset equation, which is embedded in the coefficients of the equation's kinetic terms⁴⁹⁻⁵¹.

By integrating and dropping $O(M^2)$ terms, an energy balance equation can be written as:

$$\begin{aligned} \frac{d}{dt} \left(\rho_L \dot{X}^2 + (U_k(X) + MU_M(X)) X^{\frac{D-3}{\alpha}} \right) = \\ \frac{5}{12} \left(5 - \frac{13}{3}M \right) \dot{p}_d X^{\frac{D}{\alpha}} - 4(1+M)\rho_L v_L \frac{\dot{X}^2}{X^{\frac{2}{\alpha}}} - f(\dot{M}, \ddot{M}) \end{aligned} \quad (13)$$

where $U_k(X)$ is the potential in the incompressible liquid case, defined in Eq. (4) and for $k \neq 1$:

$$U_M(X) = -\frac{40}{9}\Delta p(t)X^{\frac{3}{\alpha}} + \mu P_{GE} R_{E0}^{3k} X^{\frac{3-3k}{\alpha}} + 5SX^{\frac{2}{\alpha}} \quad (14)$$

wherein $\mu = -\frac{5}{36} \left(\frac{45k^2 - 87k + 32}{k-1} \right)$.

In the absence of the periodic driving the first term of the right-hand side vanishes. Then, for $M = 0$ the time derivative of the energy (the left-hand side) is the energy dissipated to viscosity (the second term in the right-hand side), just as expected from the motion of a damped particle in a potential.

When $M \ll 1$ and is slowly varying $\left(\frac{1}{\omega_d} \dot{M}, \frac{1}{\omega_d^2} \ddot{M} \ll 1 \right)$, the third term of the right-hand side, $f(\dot{M}, \ddot{M})$, may be neglected. Then, the left-hand side is a modified expression for a quantity that is conserved up to viscosity losses.

In this limit, which can be referred to as the adiabatic limit, it is instructive to come back to the bubble radius, R . The conserved quantity (the left-hand side of Eq. (13)) may be written, in that limit, as the product of the bubble's energy, E , and $R^{D(M)-3}$. Where the energy is

$$E = \rho_L R^3 \dot{R}^2 + U_k(R) + MU_M(R) \quad (15)$$

and by neglecting viscosity losses, we get

$$\frac{d}{dt} \left(ER^{D(M)-3} \right) = 0 \quad (16)$$

Solving for E yields:

$$E(R) = \begin{cases} E_0 \left(\frac{R}{R_0} \right)^{3-D} & \dot{R} < 0 \\ E_0 \left(\frac{R_0}{R} \right)^{D-3} & \dot{R} > 0 \end{cases} \quad (17)$$

where $E(t=0) = E_0, R(t=0) = R_0$.

Equation (17), which is valid only when M is nearly constant, i.e., when the velocity is nearly constant, leads to a remarkable observation: the energy, E , decreases both during expansion and during contraction of the bubble. This is because, during expansion the effective dimension $D(M) > 3$, while, during contraction, $D(M) < 3$.

We can use the considerations above to obtain a rough estimate of the energy loss to acoustic waves as the bubble contracts. We consider an oscillation that starts from the radius being R_{\max} , passes through the equilibrium radius R_E , and ends at the minimal radius R_{\min} . Most of the energy loss occurs in the regions of large M , which is between R_E and R_{\min} . We assume M to be constant in that region, and obtain the following estimate:

$$E_{\text{acoustic}} = \frac{4}{3} \pi (p_0 - p_V) R_{\max}^3 \left(1 - \left(\frac{R_{\min}}{R_E} \right)^{3-D} \right) \quad (18)$$

where we have assumed that the initial energy is $\frac{4}{3} \pi (p_0 - p_V) R_{\max}^3$. It is possible to deduce an approximated formula for either R_{\max} as a function of R_{\min} and R_E or R_{\min} as a function of R_{\max} and R_E by assuming conservation of energy at zeroth order in M (Eq. (C1)).

By applying (18) with $M = -0.9$ and $\lambda = 0$, for which the effective dimension is approximately 2.05, the after-bounces of the bubble were calculated with good accuracy, the result is shown in Fig. 2a. The calculation procedure is outlined in Appendix C.

V. CRITERION FOR THE REVERSAL OF THE PRIMARY BJERKNES FORCE

So far, we have examined the oscillation of a driven bubble by considering a time-dependent acoustic drive, $p_d = p_d(t)$. However, in reality, the acoustic drive also depends on position, $p_d = p_d(t, z)$.

The space-dependent drive creates a pressure gradient ∇p_d that, in turn, exert a translational force on the bubble. The primary Bjerknes force is defined as the time-averaged force over one period of the drive, given by $F_B(z) = \langle -R^3(t) \nabla p_d(t, z) \rangle^{41-44}$. For a standing acoustic wave, $p_d(t, z) = -\bar{p}_d \cos(kz) \sin(\omega_d t)$, the Bjerknes force is proportional to Φ , the time correlator:

$$\Phi \equiv -\frac{1}{2\pi R_{E0}^3} \int_0^{2\pi} R^3(\tau) \sin(\tau) d\tau \quad (19)$$

where $\tau = \omega_d t$. If $\Phi < 0$, the bubble will move toward the antinodes of the driving, while if $\Phi > 0$, it will move toward the nodes. The value of Φ is determined by the relative phase between $R(t)$ and the drive $p_d(t)$.

In the weak drive regime, $p_d \ll p_0$, the tension is negative $\Delta p < 0$ and the bubble can be approximated to oscillate in a simple harmonic potential around its ambient equilibrium radius, R_{E0} . The relative phase between the drive and the oscillation is either zero or π , depending on the relation between the bubble's internal frequency and the drive frequency⁴². If the drive frequency is higher than the internal frequency, the bubble will oscillate out-of-phase with the drive and vice versa.

The bubble's internal frequency is inversely proportional to its equilibrium radius (see Eq. (B3)). Thus, a critical radius R_C can be defined such that bubbles with a small equilibrium radius, $R_{E0} < R_C$ will oscillate out-of-phase with the drive and vice versa. The sign of Φ will then be a function of R_{E0} and R_C only.

The physical picture for *weakly* driven bubbles is now clear. Small bubbles, $R_{E0} < R_C$, will be directed to the pressure antinodes whereas big bubbles, $R_{E0} > R_C$, will be directed to the pressure nodes.

This simple description breaks down when the bubble motion deviates from the linear regime^{45,52}. As explained in Section II, when the bubble tension overcomes the tensile strength $\Delta p \geq \Delta p_c$ at some point in the acoustic cycle, strong oscillations are expected to occur. We can then calculate the time at which a small bubble ($R_{E0} < R_C$) reaches its maximum radius, which we define in dimensionless units as $\tau_{\max} = \omega_d t_{\max}$.

The shift of τ_{\max} from $\frac{\pi}{2}$ toward π , as shown in Fig. 2b, indicates a deviation from the linear regime. For weak driving, the Bjerknes force increases with the driving amplitude \bar{p}_d . However, when the driving becomes strong enough to push τ_{\max} beyond π , the positive part of the integrand in (19) increases, resulting in a decrease in the Bjerknes force.

The condition $\tau_{\max} \geq \pi$ can thus serve as a criterion for the reversal of the Bjerknes force. In Section III, we examined the bubble's expansion. The instance when the tension, $\Delta p(\tau)$, equals the tensile strength was defined as τ_* . The subsequent expansion of the bubble was approximated by Eq. (9). Differentiating it with respect to time leads to an implicit equation for the bubble's extremal points (see Eq. (D1)).

Drawing from the straightforward geometric argument provided in Appendix D, the condition $\tau_{\max} \geq \pi$ can be approximated by a relation that depends solely on the tensile strength Δp_c and the pressures:

$$\tau_* \geq \pi - \frac{\bar{p}_d}{p_0 - p_V} (1 + \cos(\tau_*)) \quad (20)$$

where $\tau_* = \arcsin\left(\frac{\Delta p_c + (p_0 - p_V)}{\bar{p}_d}\right)$.

VI. SUMMARY

We have introduced a novel perspective on the highly non-linear dynamics of a driven bubble. In the incompressible liquid regime, we developed an exact description (Eq. (3)) that is

analogous to the dynamics of a Newtonian particle in a potential. Within the compressible liquid regime, our understanding is limited to an approximate model that relies on an adiabatic treatment of the bubble's Mach number (Eq. (13)). We have demonstrated how these frameworks can be used to analytically calculate various aspects of the bubble's dynamics.

Appendix A: The Equilibrium Radius in the Isothermal Case

In Section II we derived an implicit equation for the extremal points of the bubble, as shown in Eq. (5). In the isothermal case, where $k = 1$, Eq. (5) simplifies to a cubic equation for R_E . In this appendix we show how the resulting cubic equation was *analytically* solved.

The solution to a cubic equation can be found using Cardano's method when there is one real root⁵³, and Viète's trigonometric method when there are three real roots⁵⁴. The stable equilibrium radius is the smallest positive root.

We first transform (5) to a depressed polynomial for $\sigma(t) = R_E(t) - \frac{2S}{3(p_v - p_\infty(t))}$. Then the discriminant is proportional to

$$\Delta(t) = \frac{Q_{E0}^{12} p_{GE}^2 (\Delta p - \Delta p_c)(\Delta p + \Delta p_c)}{\Delta p^4} \quad (\text{A1})$$

When $-\Delta p_c < \Delta p < \Delta p_c$ the discriminant is negative and there are three real roots. In this scenario, Viète's trigonometrical method is applied. The solution was shown in Eq. (8). Conversely, if the discriminant is positive, there is one real root and Cardano method is applied:

$$\sigma(t) = \sqrt[3]{-\frac{q}{2} + \sqrt{\Delta}} + \sqrt[3]{-\frac{q}{2} - \sqrt{\Delta}} \quad (\text{A2})$$

where $q = \frac{-2^4 S^3 + 27 \Delta p^2 p_{GE} Q_{E0}^6}{27 \Delta p^3}$. Note that when $\Delta p > \Delta p_c$, (A2) yields a negative root. This root does not correspond to a *physical* equilibrium radius.

Appendix B: Harmonic Potential Approximation

In this appendix we derive the harmonic approximation of the bubble's potential in the incompressible fluid regime (Eq. 4) around a point and explicitly write the solution for the bubble motion under a linear but time-dependent potential.

Working in the driving time scale $\tau = \omega_d t$ where $p_d(\tau) = -\bar{p}_d \sin(\tau)$, denoting $Q = Q_0 + q$ and expanding U_k to second order in q (as illustrated in Fig. 3) yields the linear equation:

$$\frac{d^2 q}{d\tau^2} = \frac{5}{2} \frac{Q_0^5}{\omega_d^2} h_B(Q_0) - \left(\frac{\omega(Q_0, \tau)}{\omega_d} \right)^2 q \quad (\text{B1})$$

where $h_B(Q)$ was defined in Eq. (2) and we have neglected

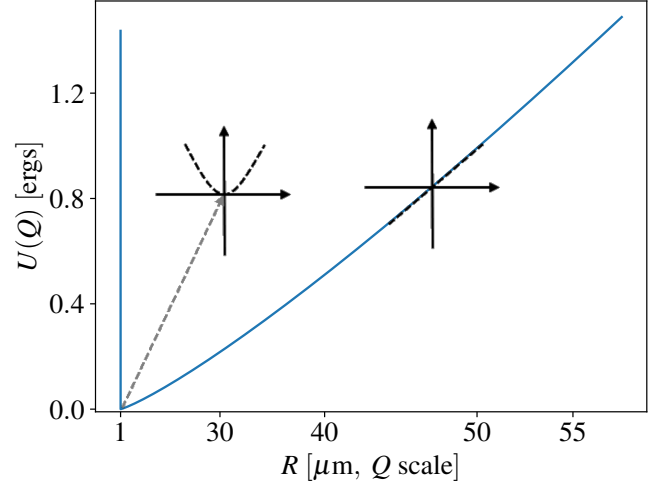


FIG. 3: Expansion of the bubble potential around a point, Q_0 . Assuming $Q = Q_0 + q$, the perturbation, q , is evolving according to $\ddot{q} = - \left(\frac{dU_k}{dq} \Big|_{q=Q_0} + \frac{d^2 U_k}{dq^2} \Big|_{q=Q_0} q \right)$. If the expansion is done far from the equilibrium point, the effective potential is approximately linear at short distances.

viscosity. The bubble's internal frequency is:

$$\omega^2(Q_0, t) = \frac{1}{2\rho_L Q_0^5} \left(\left[(6k-1) \left(\frac{Q_{E0}}{Q_0} \right)^{\frac{6k}{5}} + 1 \right] (p_0 - p_V) + p_d(t) + \frac{2S}{Q_0^3} \left[(6k-1) \left(\frac{Q_{E0}}{Q_0} \right)^{\frac{6k}{5}} - 1 \right] \right) \quad (\text{B2})$$

where Q_{E0} is the equilibrium point in the absence of the drive (referred to as the "ambient equilibrium point")

Two limiting cases can be examined, one in which the expansion point is very far from the ambient equilibrium point, $Q_0 \gg Q_{E0}$ and the second in which the two are comparable $Q_0 \sim Q_{E0}$:

$$\omega^2 \sim \frac{1}{2\rho_L Q_0^5} \begin{cases} 6k(p_0 - p_V) + p_d(t) + \frac{4(3k-1)S}{Q_0^3} & Q_0 \sim Q_{E0} \\ -\Delta p(t) & Q_0 \gg Q_{E0} \end{cases} \quad (\text{B3})$$

where surface tension was neglected for $Q_0 \gg Q_{E0}$.

The factor of $6k$ in front of the ambient and vapor pressures in the case of $Q_0 \sim Q_{E0}$ means that the driving pressure weakly affect the bubble's internal frequency around the ambient equilibrium point. This factor is absent in the case of $Q_0 \gg Q_{E0}$.

Eq. (B1) can be reduced to the linear potential case by assuming that $\omega \ll \omega_d$. Imposing initial conditions at τ_* , $Q(\tau_*) = Q_*$ and $\frac{d}{d\tau} Q(\tau_*) = v_*$ an analytical solution can be

written in terms of $\Delta\tau \equiv \tau - \tau_*$:

$$q/v_0 = -\frac{\Delta\tau^2}{2} + \left(\frac{v_*}{v_0} + \frac{\bar{p}_d/\rho_L}{\left| h_B(Q_*) + \frac{p_d}{\rho_L} \right|} \cos(\tau_*) \right) \Delta\tau - \frac{\bar{p}_d/\rho_L}{\left| h_B(Q_*) + \frac{p_d}{\rho_L} \right|} (\sin(\tau_* + \Delta\tau) - \sin(\tau_*)) \quad (\text{B4})$$

where $v_0 = \frac{5}{2} Q_*^{\frac{1}{2}} \left| h_B(Q_*) + \frac{p_d}{\rho_L} \right| / \omega_d^2$. The plus sign in front of $\frac{p_d}{\rho_L}$ results from the subtraction of $-\frac{p_d}{\rho_L}$ from the bubble's enthalpy $h_B(Q_*)$. It is crucial to acknowledge that, due to the omission of dissipation in deriving Eq. (B4), this equation does not represent a steady-state solution.

Appendix C: Collapse Extremal Points Calculation

The collapse and subsequent after-bounces extremal points are plotted as blue dots in Fig. 2a. In this appendix, we outline the method for calculating these extremal points.

First, we denote the sequence of maximal and minimal radii as $R_{\max}^{(n)}$ and $R_{\min}^{(n)}$, respectively. At the beginning of the calculation, the initial maximal radius, $R_{\max}^{(0)}$, and the equilibrium radius, R_{E0} , must be specified. Then, the initial energy is taken to be $E^{(0)} = \frac{4\pi}{3} \left(R_{\max}^{(0)} \right)^3 (p_0 - p_V)$.

Next, by assuming conservation of energy to zeroth order in M , the sequential minimal radius, $R_{\min}^{(0)}$, can be determined from Eq. (4):

$$R_{\min}^{(n)} = \left(\left(\frac{1}{k-1} \frac{p_{GE}}{p_0 - p_V} \right)^{\frac{1}{3}} \frac{R_{E0}^k}{R_{\max}^{(n)}} \right)^{\frac{1}{k-1}} \quad (\text{C1})$$

where we neglected surface tension and assumed that at $R_{\max}^{(n)}$ the internal pressure term, p_{GE} , is negligible and at $R_{\min}^{(n)}$ the tension term is negligible. The minimal radius was also constrained to be at least the van der Waals core radius.

After calculating $R_{\min}^{(n)}$, the subsequent maximal radius $R_{\max}^{(n+1)}$ must be determined. It is assumed that the bubble loses energy during its motion from its equilibrium radius to the minimal radius, as dictated by Eq. (18). This allows us to calculate $E^{(n+1)}$ from $E^{(n)}$ by specifying M . The sequential maximal radius is now obtained from energy conservation:

$$R_{\max}^{(n+1)} = R_{\max}^{(n)} \sqrt[3]{\left(\frac{R_{\min}^{(n)}}{R_{E0}} \right)^{3-D(M)}} \quad (\text{C2})$$

and we are ready to repeat the calculation. The temporal spacing between the first max and min radii was taken from the experimental data. The temporal spacing between the other extremal points was obtained from the bubble internal frequency (Eq. (B2)).

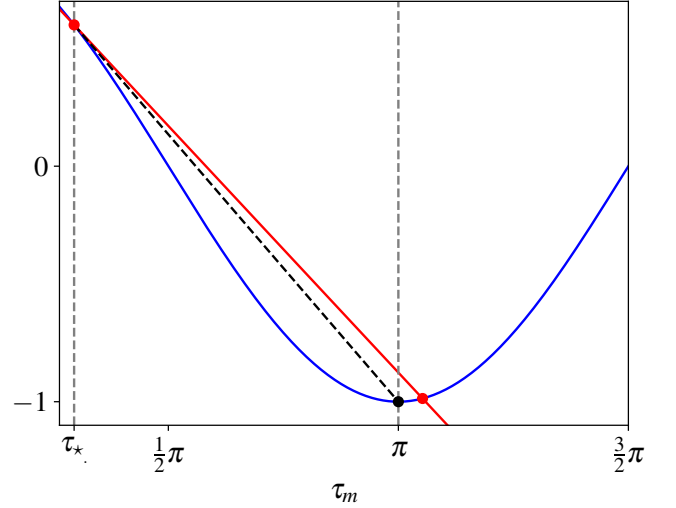


FIG. 4: Visualization of the geometric argument of Appendix D. The blue curve is the left hand side of Eq. (D1) whereas the red curve is the right hand side. The red intersection points are the solutions. The second red intersection corresponds to τ_{\max} . If the slope of the red curve exceeds that of the linear curve connecting the points $(\tau_*, \cos \tau_*)$ and $(\pi, -1)$ (represented by the black dashed line), then $\tau_{\max} > \pi$, and vice-versa.

Appendix D: Geometrical Argument for the Reversal of the Primary Bjerknes Force

In Section V, we established that Bjerknes force reversal is expected when the time it takes for the bubble to reach its maximum radius, denoted in dimensionless units as $\tau_{\max} = \omega_d t_{\max}$, exceeds π . In this appendix, we explicitly derive Eq. (20), which provides an approximation for the condition $\tau_{\max} \geq \pi$.

First, we differentiate Eq. (B4) with respect to $\tau = \omega_d t$ yielding an implicit equation for the phases at the bubble's extremal points, τ_m :

$$\cos(\tau_m) = \cos(\tau_*) - (\tau_m - \tau_*) \frac{p_0 - p_V}{\bar{p}_d} \quad (\text{D1})$$

where $\tau_* = \arcsin\left(\frac{\Delta p_c + (p_0 - p_V)}{\bar{p}_d}\right)$ and we approximated $\left| h_B(Q_*) + \frac{p_d}{\rho_L} \right| \approx \frac{p_0 - p_V}{\rho_L}$ and assumed that the velocity at τ_* is negligible, i.e., $\frac{v_*}{v_0} \ll 1$.

Eq. (D1) has two solutions between τ_* and 2π . The first solution is $\tau_m = \tau_*$ and the second solution is $\tau_m = \tau_{\max}$. The right hand side is a linear function of τ_m with $-\frac{p_0 - p_V}{\bar{p}_d}$ being the slope. The condition $\tau_{\max} \geq \pi$ is therefore equivalent to requiring that this slope will be greater or equal the slope of the linear curve connecting the points $(\tau_*, \cos \tau_*)$ and $(\pi, -1)$:

$$-\frac{p_0 - p_V}{\bar{p}_d} \geq \frac{-1 - \cos \tau_*}{\pi - \tau_*} \quad (\text{D2})$$

which is equivalent to Eq. (20). The argument is visualized in Fig. 4.

- ¹S. J. Putterman and K. R. Weninger, *Annual Review of Fluid Mechanics* **32**, 445 (2000).
- ²T. J. Matula, *Phil. Trans. R. Soc. A* **357**, 225–249 (1999).
- ³K. R. Weninger, B. P. Barber, and S. J. Putterman, *Phys. Rev. Lett.* **78**, 1799 (1997).
- ⁴T. Brennan, *Understanding Sonoluminescence* (Morgan and Claypool Publishers, 2016).
- ⁵W. Lauterborn, T. Kurz, R. Geisler, D. Schanz, and O. Lindau, *Ultrasonics Sonochemistry* **14**, 484–491 (2007).
- ⁶S. J. Putterman, *Scientific American; (United States)* **272** (1995), 10.1038/scientificamerican0295-46.
- ⁷V. Kamath, A. Prosperetti, and F. N. Egolfopoulos, *The Journal of the Acoustical Society of America* **94**, 248–260 (1993).
- ⁸R. Löfstedt, B. P. Barber, and S. J. Putterman, *Physics of Fluids A: Fluid Dynamics* **5**, 2911 (1993).
- ⁹M. P. Brenner, S. Hilgenfeldt, and D. Lohse, *Reviews of Modern Physics* **74**, 425–484 (2002).
- ¹⁰I. Akhatov, O. Lindau, A. Topolnikov, R. Mettin, N. Vakhitova, and W. Lauterborn, *Physics of Fluids* **13**, 2805–2819 (2001).
- ¹¹R. Pecha and B. Gompf, *Phys. Rev. Lett.* **84**, 1328–1330 (2000).
- ¹²O. Supponen, D. Obreschkow, P. Kobel, M. Tinguely, N. Dorsaz, and M. Farhat, *Physical Review Fluids* **2** (2017), 10.1103/physrevfluids.2.093601.
- ¹³R. E. A. Arndt, *Annual Review of Fluid Mechanics* **13**, 273–326 (1981).
- ¹⁴A. Vogel, W. Lauterborn, and R. Timm, *Journal of Fluid Mechanics* **206**, 299–338 (1989).
- ¹⁵X. Escaler, E. Egusquiza, M. Farhat, F. Avellan, and M. Coussirat, *Mechanical Systems and Signal Processing* **20**, 983–1007 (2006).
- ¹⁶E. Rambod, M. Beizaie, M. Shusser, S. Milo, and M. Gharib, *Annals of Biomedical Engineering* **27**, 774–792 (1999).
- ¹⁷J. K. Jakobsen and J. R. B. Keller, NASA Report No. NASASP-8052 (1971).
- ¹⁸L. d’Agostino, L. Torre, A. Cervone, G. Pace, D. Valentini, and A. Pasini, “An introduction to cavitation in inducers and turbopumps,” in *Cavitation Instabilities and Rotordynamic Effects in Turbopumps and Hydroturbines: Turbopump and Inducer Cavitation, Experiments and Design*, edited by L. d’Agostino and M. V. Salvetti (Springer International Publishing, Cham, 2017) pp. 1–33.
- ¹⁹D. Li, Z. Ren, Y. Li, R. Gong, and H. Wang, *Cryogenics* **116**, 103302 (2021).
- ²⁰M. Versluis, B. Schmitz, A. S. Heydt, and D. Lohse, *Science (New York, N.Y.)* **289**, 2114 (2000).
- ²¹S. N. Patek and R. L. Caldwell, *Journal of Experimental Biology* **208**, 3655–3664 (2005).
- ²²C. E. Brennen, *Interface Focus* **5**, 20150022 (2015).
- ²³J. E. Field, *Physics in Medicine and Biology* **36**, 1475–1484 (1991).
- ²⁴W. Sass, M. Bräunlich, H.-P. Dreyer, E. Matura, W. Folberth, H.-G. Priesmeyer, and J. Seifert, *Ultrasound in Medicine and amp; Biology* **17**, 239–243 (1991).
- ²⁵L. Biasiori-Poulanges, B. Lukić, and O. Supponen, *Ultrasonics Sonochemistry* **102**, 106738 (2024).
- ²⁶T. Yu, Z. Wang, and T. J. Mason, *Ultrasonics Sonochemistry* **11**, 95–103 (2004).
- ²⁷M. Dular, T. Griessler-Bulc, I. Gutierrez-Aguirre, E. Heath, T. Kosjek, A. Krivograd Klemenčič, M. Oder, M. Petkovšek, N. Rački, M. Ravnikar, A. Šarc, B. Širok, M. Zupanc, M. Žitnik, and B. Kompare, *Ultrasonics Sonochemistry* **29**, 577–588 (2016).
- ²⁸Y. Song, R. Hou, W. Zhang, and J. Liu, *Water Science and Technology* **86**, 302–320 (2022).
- ²⁹W. D. Song, M. H. Hong, B. Lukyanchuk, and T. C. Chong, *Journal of Applied Physics* **95**, 2952–2956 (2004).
- ³⁰A. B. Basset, *A Treatise on Hydrodynamics* (Cambridge University Press, 1888).
- ³¹L. Rayleigh, *The London, Edinburgh, and Dublin Philosophical Magazine and Journal of Science* **34**, 94 (1917).
- ³²M. S. Plesset, *Journal of Applied Mechanics* **16**, 277 (1949).
- ³³C. E. Brennen, *Cavitation and Bubble Dynamics* (Cambridge University Press, 2013).
- ³⁴T. G. Leighton, *The Acoustic Bubble* (Elsevier, 1994).
- ³⁵A. Prosperetti and A. Lezzi, *Journal of Fluid Mechanics* **168**, 457 (1986).
- ³⁶J. B. Keller and I. I. Kolodner, *Journal of Applied Physics* **27**, 1152 (1956).
- ³⁷D. Epstein and J. B. Keller, *The Journal of the Acoustical Society of America* **52**, 975 (1972).
- ³⁸J. B. Keller and M. Miksis, *The Journal of the Acoustical Society of America* **68**, 628 (1980).
- ³⁹C. Herring, *Theory of the pulsations of the gas bubble produced by an underwater explosion* (Columbia Univ., Div. of National Defense Research, New London, Conn, 1941, 1941).
- ⁴⁰L. Trilling, *Journal of Applied Physics* **23**, 14 (1952).
- ⁴¹V. Bjerknes, *Fields of Force* (Columbia University Press, 1906).
- ⁴²T. G. Leighton, A. J. Walton, and M. J. W. Pickworth, *European Journal of Physics* **11**, 47–50 (1990).
- ⁴³L. A. Crum, *The Journal of the Acoustical Society of America* **57**, 1363 (1975).
- ⁴⁴O. Louisnard, *Physical Review E* **78** (2008), 10.1103/physreve.78.036322.
- ⁴⁵I. Akhatov, R. Mettin, C. D. Ohl, U. Parlitz, and W. Lauterborn, *Physical Review E* **55**, 3747–3750 (1997).
- ⁴⁶D. R. Childs, *International Journal of Non-Linear Mechanics* **8**, 371–379 (1973).
- ⁴⁷C. Hunter, *Journal of Fluid Mechanics* **8**, 241–263 (1960).
- ⁴⁸D. Obreschkow, M. Bruderer, and M. Farhat, *Physical Review E* **85** (2012), 10.1103/physreve.85.066303.
- ⁴⁹A. R. Klotz, *Physics of Fluids* **25** (2013), 10.1063/1.4817803.
- ⁵⁰N. A. Kudryashov and D. I. Sinelshchikov, *Physics Letters A* **379**, 798–802 (2015).
- ⁵¹Z. Wang, Y. Qin, and L. Zou, in *AIP Conference Proceedings* (Author(s), 2018).
- ⁵²T. J. Matula, S. M. Cordry, R. A. Roy, and L. A. Crum, *The Journal of the Acoustical Society of America* **102**, 1522–1527 (1997).
- ⁵³S. Gindikin, “Ars magna (the great art),” in *Tales of Mathematicians and Physicists* (Springer New York, New York, NY, 2007) pp. 1–26.
- ⁵⁴R. W. D. Nickalls, *The Mathematical Gazette* **90**, 203–208 (2006).